Resonant Raman scattering in quasi-two-dimensional InSe near the M_0 and M_1 critical points

Shalini Ashokan* and K. P. Jain
Laser Technology Research Programme, Indian Institute of Technology, New Delhi 110016, India

M. Balkanski and C. Julien
Laboratoire de Physique des Solides, Université Pierre et Marie Curie, 4 place Jussieu, 75230 Paris CEDEX 05, France

(Received 1 April 1991)

A theory of Raman scattering in quasi-two-dimensional crystals is presented, emphasizing resonance enhancement at the excitonic transition appropriate to the M_0 and M_1 edges. The effect of electron-hole Coulomb interaction leads to metamorphism of the critical points. Our experimental results on quasi-two-dimensional InSe crystal show double resonant structure for both incident- and scattered-photon energies near the direct exciton energy. The theory provides a good fit to the experiments both above and below the excitonic transition after inclusion of the electron-hole interaction.

I. INTRODUCTION

InSe and GaSe belong to the group of III-VI semiconductors in which each layer[1] is structurally identical and composed of selenium atoms on either side of a double plane of gallium or indium atoms. The large difference in the relative strength of the intralayer and interlayer forces leads to quasi-two-dimensional[2,3] character of GaSe and InSe. InSe forms in the same three different polytypes[4] as GaSe.

The lowest direct and indirect band gaps[5] in InSe are at 1.256 and 1.187 eV, respectively, at 300 K. According to Abutalybov and Belle,[6] the low-energy side of the absorption spectrum corresponds to a hyperbolic exciton formed near the M_1 saddle point. The energy of the M_1 edge in InSe is 2.77 eV at 300 K, and the binding energy of the hyperbolic exciton was found to be 0.35 eV.

The vibrational properties of InSe have been studied[7-10] by infrared and Raman spectroscopy. The Raman investigations exhibit polar, nonpolar, and second-order phonon modes of InSe.

Resonant Raman-scattering (RRS) studies in InSe near the excitonic transition have been reported[11-13] in the literature. These experimental results were compared with simple theories[14,15] appropriate to three-dimensional Van Hove singularities. The nature of the singularities is, however, dimension dependent and quite different in two dimensions. It is therefore worthwhile to formulate a theory of RRS at critical points in two-dimensional semiconductors, taking into account the dimensionality-related aspects in Raman scattering (RS), particularly the resonant nature of the intermediate scattering states.

In this paper we present a theory of RRS at M_0 and M_1 critical points of two-dimensional semiconductors for free electron-hole (e-h) pairs as intermediate scattering states. This theory is extended to incorporate e-h Coulomb interaction. The calculated Raman amplitude shows a double-resonance structure corresponding to incoming and outgoing photon resonance near the continuum (M_0, M_1 edges) for the noninteracting case.

A more realistic treatment of the Coulomb e-h interaction leads to metastable (hyperbolic) exciton resonances near the M_1 edge. A typical double-resonance structure associated with these resonances appears in the Raman-scattering amplitude. In addition to resonance scattering, scattering in the continuum states takes place near the M_0 and M_1 edges. The effect of the e-h interaction is to broaden the resonance structure and smear out the singularity between ω_g and $\omega_g+\omega_0$. This leads to the metamorphism of the critical points.

We also present our experimental results on RRS in a quasi-two-dimensional InSe layered semiconductor near the excitonic transition energy stressing the resonance nature of the scattering process. In InSe we have observed the double-resonance effect. Our experimental results agree well with the theory both below and above the excitonic transition energy after including the e-h interaction. Comparison between experimental results and theoretical calculations shows that hyperbolic excitons in InSe act as the intermediate scattering state.

II. THEORY OF RAMAN SCATTERING NEAR THE VAN HOVE SINGULARITY: M_0 EDGE

A. Free electron-hole pairs

Consider Raman scattering in two-dimensional (2D) crystals near the M_0 edge assuming free electron-hole (e-h) pairs as intermediate scattering states. The Raman amplitude in two dimensions at the M_0 edge analogous to that in three dimensions[16] is

$$A(\omega)\simeq\int_0^{K_{\max}} d^2k_\rho \frac{1}{(\omega_k-\omega+i\Gamma)(\omega_k-\omega+\omega_0+i\Gamma)}\ , \tag{1}$$

where k_ρ is the 2D wave vector. Γ is the damping factor associated with the lifetime of the intermediate scattering states. ω and ω_0 are the energies of the incident and scattered phonons, respectively. The momentum dependence

of the scattering matrix elements has been neglected in Eq. (1).

Assuming parabolic bands,

$$\omega_k = \omega_g + \frac{hk_\rho^2}{2m} , \tag{2}$$

where ω_g is band gap at the M_0 point. Thus Eq. (1) becomes

$$A(\omega) \simeq \int_0^{K_{\max}} d\omega_k \frac{1}{(\omega_k - \omega + i\Gamma)(\omega_k - \omega + \omega_0 + i\Gamma)} . \tag{3}$$

Simple integration of Eq. (3) gives the Raman amplitude at the M_0 edge as

$$A(\omega) \simeq \frac{1}{\omega_0}[\ln(x_1^2+y_1^2)^{1/2} - \ln(x_2^2+y_2^2)^{1/2}] + \frac{i}{\omega_0}\left[\tan^{-1}\left[\frac{y_1}{x_1}\right] - \tan^{-1}\left[\frac{y_2}{x_2}\right]\right] , \tag{4}$$

for all values of ω, where

$$x_1 = \frac{\omega^2+\Gamma^2-\omega\omega_g}{\Gamma^2+\omega^2}, \quad y_1 = \frac{-\Gamma\omega_g}{\Gamma^2+\omega^2} ,$$

$$x_2 = \frac{\omega^2+\Gamma^2-\omega\omega_g+(\omega_g-2\omega)\omega_0}{(\omega_0-\omega)^2+\Gamma^2} ,$$

$$y_2 = \frac{-\Gamma\omega_g}{(\omega_0-\omega)^2+\Gamma^2} .$$

Similarly, scattering at the M_3 edge can be calculated by using a negative effective mass, so that

$$\omega_k = \omega_g - \frac{h}{2m}k_\rho^2 . \tag{5}$$

Hence the results at the M_3 edge are the same as for the M_0 edge, but with a negative sign.

B. Exciton effects: Coulomb interaction

So far, the interaction between the electron and hole has been neglected. We have used Coulomb interaction to incorporate the effect of *e-h* interaction, which is more realistic than the Slater-Koster interaction and gives an adequate description of discrete and resonance levels.

The Coulomb interaction is distinguished by two important properties:[17] (i) It is weak when connecting Bloch pair states from different bands or distant regions in momentum space. (ii) It is singularly strong for a small momentum-transfer process within a single band.

According to the first property, the effective-mass approximation gives the excitonic effects correctly. The second property reflects a rather singular behavior of the solution of the effective-mass equation. The effective-mass equation[17] can be written as

$$\left[\frac{1}{2m}\left[\frac{\partial^2}{\partial x^2}+\frac{\partial^2}{\partial y^2}\right] + \frac{1}{\epsilon(x^2+y^2+z^2)^{1/2}} + E\right]\phi(x,y,z) = 0 , \tag{6}$$

with the condition $m_1 = m_2 = m < 0$, $m_3 > 0$, where ϵ is the dielectric constant of the crystal, m is the reduced mass of the electron and hole, and $\phi(x,y,z)$ is the envelope function of Wannier exciton. E is the energy eigenvalue measured from the bottom of the conduction band.

The eigenfunctions have the form

$$\Phi = \phi(x,y;\xi)\delta(z-\xi) , \tag{7}$$

where ϕ is the solution obtained from Eq. (6). After substituting $z=0$ in Eq. (6) the Schrödinger equation (6) reduces to a "two-dimensional hydrogen atom" and the solution of the equation contains discrete as well as continuous solutions. It is known that at the M_0 edge, the principal effective mass has two positive components. Hence Eq. (6) will give the exact solution at the M_0 edge. The solution of Eq. (6) results in bound states with binding energies

$$E_n(0) = \frac{2m}{\epsilon^2(2n-1)^2}, \quad n = 1,2,\ldots . \tag{8}$$

The value of the envelope function for these resonant states are

$$|\phi_n(0)|^2 = \frac{16m^3}{\pi\epsilon^3(2n-1)^3} , \tag{9}$$

and for the continuum states,

$$|\phi_E(0)|^2 = \frac{\exp(-\gamma)}{\cosh\gamma} , \tag{10}$$

where

$$\gamma = -\pi|E_n(0)|^{1/2}/2(\omega-\omega_g)^{1/2} ,$$

and ω_g is the M_0 point energy. Equation (1), the Raman amplitude, therefore becomes

$$A(\omega) \simeq \sum_n \frac{16m^3}{\pi\epsilon^3(2n-1)^3} \frac{1}{[\omega_g-\omega-|E_n(0)|+i\Gamma][\omega_g-\omega+\omega_0-|E_n(0)|+i\Gamma]} + \int_0^{k_{\max}} d^2k_\rho \frac{|\phi_E(0)|^2}{(\omega_k-\omega+i\Gamma)(\omega_k-\omega+\omega_0+i\Gamma)} . \tag{11}$$

Here $|\phi_E(0)|^2$ is the envelope function of the exciton in the continuum state.

Using Eqs. (2) and (10), Eq. (11) becomes

$$A(\omega)\simeq\sum_n \frac{16m^3}{\pi\epsilon^3(2n-1)^3}\,\frac{1}{[\omega_g-\omega-|E_n(0)|+i\Gamma][\omega_g-\omega+\omega_0-|E_n(0)|+i\Gamma]}$$
$$+\int_0^{k_{\max}} d\omega_k \frac{(1-\tanh\gamma)}{(\omega_k-\omega+i\Gamma)(\omega_k-\omega+\omega_0+i\Gamma)} \,. \tag{12}$$

Taking the upper limit of the above integral as $|K_{\max}|=\infty$, the integral can be evaluated with the help of contour shown previously.[18] The first term of the integral is the no *e-h* term given by Eq. (4). The value of the integral for all values of ω is evaluated as

$$\text{No } e\text{-}h \text{ term[given by Eq.(4)]}+\frac{1}{\omega_0}\left[\tan\left[A\frac{\sin\theta_1}{[(\omega-\omega_g)^2+\Gamma^2]^{1/4}}\right]-\tan\left[A\frac{\sin\theta_2}{[(\omega-\omega_0-\omega_g)^2+\Gamma^2]^{1/4}}\right]\right]$$
$$+\frac{i}{\omega_0}\left[\tanh\left[A\frac{\cos\theta_2}{[(\omega-\omega_0-\omega_g)^2+\Gamma^2]^{1/4}}\right]-\tanh\left[A\frac{\cos\theta_1}{[(\omega-\omega_g)^2+\Gamma^2]^{1/4}}\right]\right], \tag{13}$$

where

$$\theta_1=\frac{1}{2}\tan^{-1}\frac{\Gamma}{\omega-\omega_g},\quad \theta_2=\frac{1}{2}\tan^{-1}\frac{\Gamma}{\omega-\omega_0-\omega_g},\quad A=-\frac{\pi|E_1(0)|^{1/2}}{2}\,.$$

For incident-photon energies in the vicinity of the exciton energy, the contribution from the discrete state is dominant and the amplitude becomes

$$A(\omega)\simeq\sum_n \frac{16m^3}{\pi\epsilon^3(2n-1)^3}\,\frac{1}{[\omega_g-\omega-|E_n(0)|+i\Gamma][\omega_g-\omega+\omega_0-|E_n(0)|+i\Gamma]}\,. \tag{14}$$

For photon energies far away from the metastable resonant energies, the Raman amplitude is given by Eq. (13). Figure 1 shows the Raman intensity of a typical two-dimensional semiconductor GaSe at the M_0 edge. The dashed line corresponds to the noninteracting *e-h* pair and is evaluated using Eq. (4) with $h\omega_g=2.06$ eV, $h\omega_0=30$ meV, and $h\Gamma=5$ meV. The solid line is obtained by considering the Coulomb interaction between an *e-h* pair and is evaluated using Eqs. (12) and (13) taking $|E_1(0)|=0.05$ eV and $\epsilon=6.5$.

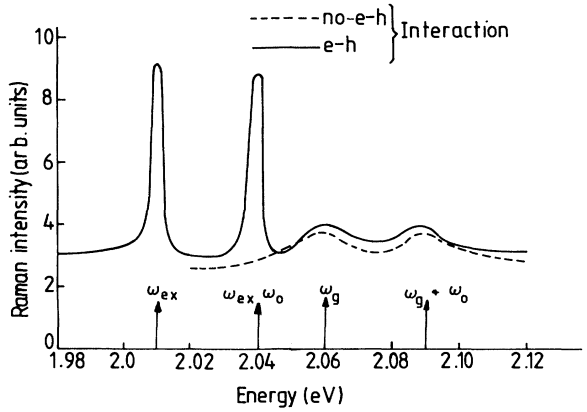

FIG. 1. First-order Stokes-Raman spectrum of a typical 2D semiconductor at the M_0 edge. The dashed line corresponds to noninteracting *e-h* pairs. The solid line is obtained by considering Coulomb correlated *e-h* pairs. The fitting parameters are described in the text.

The value of constant C has been chosen arbitrarily in both cases. The noninteracting case shows a double-resonance behavior corresponding to incoming and outgoing photon resonances near the continuum (M_0 edge). Resonance enhancement is observed near the discrete hydrogenic exciton energies. In addition to the resonance scattering, scattering due to the continuum states also takes place near the M_0 edge. The sharp nature of the resonance scattering (ω_{ex} and $\omega_{ex}+\omega_0$) due to hydrogenic excitons is evident from Fig. 1. Furthermore, it is clearly seen in Fig. 1 that the effect of *e-h* interaction on Raman amplitude is rather weak near the singularity (M_0 edge). At the M_3 edge, the principal effective masses are negative and the Coulomb interaction behaves as a repulsive interaction. Thus no bound states appear.

III. THEORY OF RAMAN SCATTERING NEAR THE SADDLE-POINT SINGULARITY: M_1 EDGE

A. Free electron-hole pairs

Equation (1) can also be written in 2D as

$$A(\omega)\simeq\int_0^{k_{\max}} dk_x\,dk_y \frac{1}{(\omega_k-\omega+i\Gamma)(\omega_k-\omega+\omega_0+i\Gamma)}\,. \tag{15}$$

For the M_1 saddle point in 2D, we assume

$$\omega_k=\omega_g+\frac{h(k_x^2-k_y^2)}{2m}\,, \tag{16}$$

where k_x and k_y are the wave vectors in the x-y plane. Equation (16) has been written in the above form to take

into account the signs of the effective masses along the different principal directions. It is known that at the M_1 saddle point the principal effective mass has one positive and one negative component.

Then Eq. (15) can be written as

$$A(\omega)\simeq\int_0^{k_{\max}}\frac{(\omega_k-\omega_g)^{-1/2}(k_{y\max}-k_{y\min})}{(\omega_k-\omega+i\Gamma)(\omega_k-\omega+\omega_0+i\Gamma)}d\omega_k \ . \tag{17}$$

From Eq. (16) one sees that

$$k_{y\min}=\begin{cases}0 & \text{if } \omega_k>\omega_g\\ \dfrac{2m(\omega_g-\omega_k)^{1/2}}{h^2} & \text{if } \omega_k<\omega_g \ .\end{cases} \tag{18}$$

Since $k_{y\max}$ is constant, it is replaced by K. The second term of Eq. (17) will be a slowly varying function of ω near ω_g, which we call C (a constant). Therefore, Eq. (17) becomes

$$A(\omega)\simeq -C+K\int_{\omega_g}^{\infty}\frac{(\omega_k-\omega_g)^{-1/2}}{(\omega_k-\omega+i\Gamma)(\omega_k-\omega+\omega_0+i\Gamma)}d\omega_k \ . \tag{19}$$

The above integral will be evaluated with the help of the same contour discussed in Sec. II. The poles are at $\omega_k=\omega-i\Gamma$ and $\omega_k=\omega-\omega_0-i\Gamma$. Then the Raman amplitude at the M_1 edge for free e-h pairs for all values of ω becomes

$$A(\omega)\simeq -C+\frac{K}{\omega_0}\left[\frac{\sin\theta_2}{[(\omega-\omega_0-\omega_g)^2+\Gamma^2]^{1/4}}-\frac{\sin\theta_1}{[(\omega-\omega_g)^2+\Gamma^2]^{1/4}}\right]+\frac{iK}{\omega_0}\left[\frac{\cos\theta_1}{[(\omega-\omega_g)^2+\Gamma^2]^{1/4}}-\frac{\cos\theta_2}{[(\omega-\omega_0-\omega_g)^2+\Gamma^2]^{1/4}}\right], \tag{20}$$

where

$$\theta_1=\frac{1}{2}\tan^{-1}\left[\frac{\Gamma}{\omega-\omega_g}\right]$$

and

$$\theta_2=\frac{1}{2}\tan^{-1}\left[\frac{\Gamma}{\omega-\omega_0-\omega_g}\right] .$$

B. Exciton effects: Coulomb interaction

Coulomb interaction between e-h pairs at the saddle point leads to metastable (hyperbolic) excitons. The nature of energy surfaces are different at the saddle point which will complicate the theory of metastable excitons. A possible theoretical approach to the theory of metastable excitons is in the literature.[17,19] We, however, approach this problem using the method of separation in parabolic coordinates.[20] The two-dimensional hydrogen-atom effective-mass equation with Coulomb potential can be written as

$$\left[-\frac{h^2}{2m_1}\frac{\partial^2}{\partial x^2}-\frac{h^2}{2m_2}\frac{\partial^2}{\partial y^2}-\frac{1}{\epsilon r}\right]\psi(x,y)=E\psi(x,y) \ , \quad E<0 \ . \tag{21}$$

For a Coulomb field, the separation of variables can be written in parabolic coordinates, which are defined as

$$x=(\xi\eta)^{1/2}\cos\phi, \quad y=(\xi\eta)^{1/2}\sin\phi \ ,$$
$$Z=\tfrac{1}{2}(\xi-\eta), \quad r=(x^2+y^2+z^2)^{1/2}=\tfrac{1}{2}(\xi+\eta) \ ,$$

or, conversely,

$$r=\tfrac{1}{2}(\xi+\eta), \quad \xi=r+z, \quad \eta=r-z \ . \tag{22}$$

The principal effective mass at the M_1 saddle point in 2D has one positive and one negative component so that the effective-mass equation in parabolic coordinates can be written as

$$\frac{h^2}{2m_1}\frac{4}{\xi+\eta}\frac{\partial}{\partial\xi}\left[\xi\frac{\partial\psi}{\partial\xi}\right]-\frac{h^2}{2m_2}\frac{4}{\xi+\eta}\frac{\partial}{\partial\eta}\left[\eta\frac{\partial\psi}{\partial\eta}\right]+\frac{2}{\epsilon(\xi+\eta)}\psi=|E|\psi \ . \tag{23}$$

The separation is accomplished by substituting

$$\psi(\xi,\eta)=f_1(\xi)f_2(\eta) \ , \tag{24}$$

so that Eq. (24) can be separated into ξ and η:

$$\frac{1}{f^1}\frac{d}{d\xi}\left[\xi\frac{df_1}{\xi}\right]+\frac{m_1}{\epsilon h^2}-\frac{m_1|E|\xi}{2h^2}=\frac{1}{f_2}\frac{d}{d\eta}\left[\eta\frac{df_2}{d\eta}\right]+\frac{m_2|E|\eta}{2h^2}=v \ , \tag{25}$$

where v is the separation constant and is determined by the boundary conditions. Thus the equations for f_1 and f_2 are

$$\frac{d}{d\xi}\left[\xi\frac{df_1}{d\xi}\right]-\left[\frac{m_1|E|\xi}{2h^2}-\frac{m_1}{\epsilon h^2}+v\right]f_1=0 \tag{26}$$

and

$$\frac{d}{d\eta}\left[\eta\frac{df_2}{d\eta}\right]-\left[v\frac{m_2|E|\eta}{2h^2}\right]f_2=0 \ . \tag{27}$$

With the condition $m_2^{-1}=0$ and $m_1=m<0$, only Eq. (26) will contribute to the solution. Therefore, the energy levels may be determined by substituting $y=\alpha\xi$, so that Eq. (26) becomes

$$\frac{1}{y}\frac{d}{dy}\left[y\frac{df_1}{dy}\right]+\left[\frac{\lambda_1}{y}-\frac{1}{4}\right]f_1=0 \ , \tag{28}$$

where

$$\alpha^2=\frac{2m|E|}{h^2} \tag{29}$$

and

$$\lambda_1=\frac{1}{\alpha}\frac{m}{\epsilon h^2} . \tag{30}$$

The asymptotic behavior is dominated by the factor $e^{\pm 1/2y}$, where we must take the negative sign in the exponent. Substituting $f_1(y)=e^{-1/2y}L(y)$ into Eq. (28), we obtain an equation for L:

$$yL''+(1-y)L'+(\lambda_1-\tfrac{1}{2})L=0 . \tag{31}$$

The terminating solutions are the associated Laguerre polynomials and they are $L_{n_1}(y)$, where

$$n_1=\lambda_1-\tfrac{1}{2} \tag{32}$$

is a positive integer of zero. Combining Eqs. (28), (29), and (31), the energy levels are given by

$$E_{n_1}=|-E_{n_1}|=-\frac{2m}{\epsilon^2(2n_1+1)^2} , \tag{33}$$

and the normalized wave function for a two-dimensional[21] hydrogen atom is given by

$$\psi^0_{n_1 m}(r)=\left[\frac{n_1-|m|!}{\pi a^2(n_1+\frac{1}{2})^3[(n_1+|m|!)]^3}\right]^{1/2} \times e^{-1/2\rho}\rho^{|m|}L^{2|m|}_{(n_1+|m|)}(\rho)e^{im\phi} , \tag{34}$$

where $r(\xi,\eta,0)$ is denoted by r, $\rho=r/a\lambda$, $a=\epsilon h^2/m$, and $\lambda_1=n_1+\frac{1}{2}$.

Thus the corresponding wave functions in our case will be

$$|\psi_1(0)|^2=\frac{8m^2}{\pi\epsilon^2(2n_1+1)^3} . \tag{35}$$

We know that the Schrödinger equation in two dimensions is given by Eq. (6), and so one can calculate its solutions for a finite mass m_2. This can be done by the adiabatic approximation. We therefore put

$$\Phi(x,y)=\psi_n(x;y)\phi_n(y) , \tag{36}$$

where ψ is the solution of Eq. (21) and ϕ is to be found from the one-dimensional equation

$$\left[-\frac{1}{2m_2}\frac{\partial^2}{\partial y^2}+E_n\right]\phi(y)=E\phi(y) , \tag{37}$$

which also gives the energy spectrum. The function E is the potential energy for the "particle" m_2, if $m_2>0$, and is given by Eq. (33). The WKBJ estimate (which cannot be applied for energies close to the top of the barrier) gives the line shape using the WKB approximation.

Then the corresponding analytic expressions are, for $E>E_n(-2m/9\epsilon^2)$,

$$|\phi_E(0)|^2=|\psi_1(0)|^2\left[\frac{|m_2|}{m}\left[\frac{\epsilon^2}{2m}E+1\right]\right]^{-1/2} , \tag{38}$$

and for $E<E_n(-2m/9\epsilon^2)$,

$$|\phi_E(0)|^2=|\psi_1(0)|^2\left[\frac{|m_2|}{m}\left[\frac{\epsilon^2}{2m}E+1\right]\right]^{-1/2} \times\exp\left[-\frac{1}{3}\left[\frac{|m_2|}{m}\right]^{1/2}\left[\frac{\epsilon^2}{2m}E+1\right]^{3/2}\right] . \tag{39}$$

The results are similar to that of Velický and Sak. As $|m_2|^{-1}$ increases, the adiabatic approximation becomes valid, and the intensity of these singularities, rapidly decreases. With the help of Eqs. (11), (17), and (39), the Raman amplitude for interacting e-h pairs at the M_1 edge can be written as

$$A(\omega)\simeq\sum_n\frac{8m^2}{\pi\epsilon^2(2n_1+1)^3}\frac{1}{[\omega_g-\omega-|E_n(0)|+i\Gamma][\omega_g-\omega+\omega_0-|E_n(0)|+i\Gamma]} + K\int_{\omega_g}^{\infty}d\omega_k\frac{(\omega_k-\omega_g)^{-1/2}\left[\frac{|m_2|}{m}\left[\frac{\epsilon^2}{2m}\omega_k+1\right]\right]^{-1/2}\exp\left[\frac{1}{3}\left[\frac{|m_2|}{m}\right]^{1/2}\left[\frac{\epsilon^2\omega_k}{2m}+1\right]^{3/2}\right]}{(\omega_k-\omega+i\Gamma)(\omega_k-\omega_0+i\Gamma)} , \tag{40}$$

where $\omega_k=E_k/h$ and the Raman amplitude h is taken as unity. The value of the integral is evaluated and the Raman amplitude becomes, at the M_1 edge,

$$\begin{aligned}A(\omega)\simeq{}&C+\text{no } e\text{-}h \text{ term [given by Eq. (20)]}+\frac{A}{\omega_0}\left[\frac{1}{[\omega_g-\omega-|E_n(0)|+i\Gamma]}-\frac{1}{[\omega_g-\omega+\omega_0-|E_n(0)|+i\Gamma]}\right]\\&+\frac{iKA}{B\omega_0}(T\cos\theta_1\cos\theta_2\sin\theta_3-T\sin\theta_1\cos\theta_2\cos\theta_3+T\sin\theta_2\cos\theta_1\cos\theta_3+T\sin\theta_1\sin\theta_2\sin\theta_3-T'\cos\theta_1'\cos\theta_2'\sin\theta_3'\\&\quad-T'\sin\theta_1'\cos\theta_2'\cos\theta_3'-T'\sin\theta_2'\cos\theta_1'\cos\theta_3'-T'\sin\theta_1'\sin\theta_2'\sin\theta_3')\\&+\frac{KA}{B\omega_0}(T\cos\theta_1\cos\theta_2\cos\theta_3+T\sin\theta_1\sin\theta_2\cos\theta_3+T\sin\theta_1\cos\theta_2\sin\theta_3-T\cos\theta_1\sin\theta_2\sin\theta_3\\&\quad-T'\cos\theta_1'\cos\theta_2'\cos\theta_3'-T'\sin\theta_1'\sin\theta_2'\cos\theta_3'+T'\sin\theta_1'\cos\theta_2'\sin\theta_3'+T'\cos\theta_1'\sin\theta_2'\sin\theta_3') ,\end{aligned} \tag{41}$$

for all values of ω. Here

$$A=\frac{8m^2}{\pi\epsilon^2(2n_1+1)^3},$$

$$B=\left[\frac{|m_2|}{m}\right]^{1/2},$$

$$A'=\exp[-B/3r_2^{3/2}\cos(3\theta_2)],$$

$$T=r_1^{-1/2}r_2^{-1/2}A',$$

$$r_1=[(\omega_g-\omega)^2+\Gamma^2]^{1/2},$$

$$r_2=[(C\omega+1)^2+(C\Gamma)^2]^{1/2},$$

$$C=\epsilon^2/2m,$$

$$\theta_1=\frac{1}{2}\tan^{-1}\frac{\Gamma}{\omega_g-\omega},\quad \theta_2=\frac{1}{2}\tan^{-1}\frac{C\Gamma}{C\omega+1},$$

$$\theta_3=B/3r_2^{3/2}\sin(3\theta_2),$$

$$T'=r_1'^{-1/2}r_2'^{-1/2}A'',$$

$$r_1'=[(\omega_g-\omega+\omega_0)^2+\Gamma^2]^{1/2},$$

$$r_2'=[(C\omega-C\omega_0+1)^2+(C^2\Gamma^2)]^{1/2},$$

$$A''=\exp(-B/3r_2'^{3/2}\cos3\theta_2'),$$

$$\theta_1=\frac{1}{2}\tan^{-1}\frac{\Gamma}{\omega_g+\omega_0-\omega},\quad \theta_2=\frac{1}{2}\tan^{-1}\frac{C\Gamma}{C\omega-C\omega_0+1},$$

and

$$\theta_3'=[B/3r_2'^{3/2}\sin(3\theta_2')].$$

Figure 2 shows the Raman intensity of a typical two-dimensional semiconductor at the M_1 edge. The dashed line corresponds to the noninteracting case. $A(\omega)$ is given by Eq. (20) for the M_1 edge. The solid line represents the effect of *e-h* interaction and is obtained using Eqs. (40) and (41). The damping factor is chosen as $\Gamma=5$ meV for both cases. The noninteracting case shows a double resonance corresponding to incoming and outgoing photon resonances near the continuum (M_1 edge). Incorporation of the *e-h* interaction via the Coulomb potential leads to metastable (hyperbolic) exciton resonances near the M_1 edge. Typical resonance structures associated with these resonances appear (ω_{ex} and $\omega_{ex}+\omega_0$) in the RRS amplitude. This is analogous to the resonant scattering owing to hydrogenic excitons near the M_0 edge, as discussed in Sec. II. In addition to this resonance, scattering due to continuum states takes place near the M_1 edge. This situation is similar to that of the dual relationship between the local and band aspects, which results in the metamorphosis of the critical points.[17,22] The effect of the *e-h* is to broaden the resonance curve and smear the singularity between ω_g and $\omega_g+\omega_0$. At the M_1 edge (Fig. 2), the effect of the *e-h* interaction is more prominent compared to the M_0 edge (Fig. 1) because of the nature of the singularity.

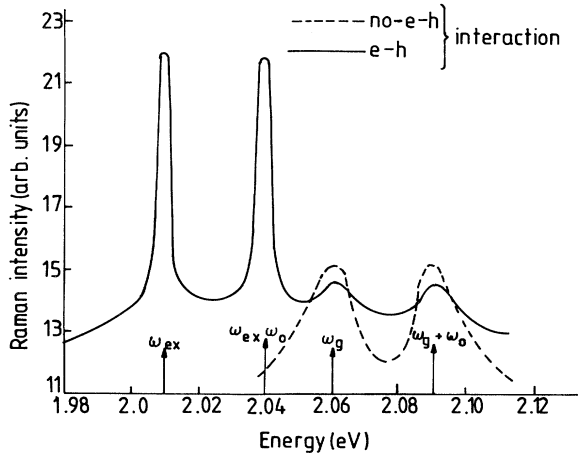

FIG. 2. First-order Stokes-Raman spectrum of a typical 2D semiconductor at the M_1 edge. The dashed line corresponds to noninteracting *e-h* pairs. Coulomb interaction is used to incorporate the effect of *e-h* pairs and is represented by solid line. The fitting parameters are described in the text.

IV. EXPERIMENTAL PROCEDURE

A single crystal of InSe was grown by using the modified Bridgman technique from high-purity elements.

Resonant Raman-scattering experiments were done in the backscattering geometry using standard techniques. The scattered light was analyzed by a double monochromator and the signal detected by photon-counting electronics.

Resonance near the excitonic transition energy was studied by using various lines of an argon-ion laser and temperature tuning the gap.[23] For temperature tuning the gap, the samples were mounted in a closed-cycle cryostat and the temperature was accurately measured using a calibrated gold-Chromel thermocouple. The incident laser power was kept below 100 mW to avoid sample heating effects. The lifetime broadening of the phonon modes does not vary appreciably with the temperature, and hence the damping factor is constant in this temperature range. The absorption-corrected Raman efficiency was normalized to the 520-cm^{-1} line of silicon, which takes care of the ω^4 dependence.

V. RESULTS AND DISCUSSION

Figure 3 shows the resonance Raman spectrum at 77 K of Bridgman-grown InSe using the $\lambda=4880$ Å line in the backscattering geometry. The main features observed here are at 180, 203, 213, 230, 406, 412, and 430 cm^{-1}. The first-order phonons are observed between 100 and 200 cm^{-1} and the second-order spectrum extends from 380 to 450 cm^{-1}. In Table I the observed phonons are listed along with other published results.[9] The features at 203 and 213 cm^{-1} were originally assigned to E'(TO) and E'(LO) modes, and their presence implies[7] ε-polytype. In fact, the total number of five modes in the first-order spectrum also confirms the ε-polytype nature. The sixth mode, expected at 17 cm^{-1}, could not be observed because of Rayleigh diffusion. The modes at 118, 180, and 230 cm^{-1} are the nonpolar modes and the modes at 203,

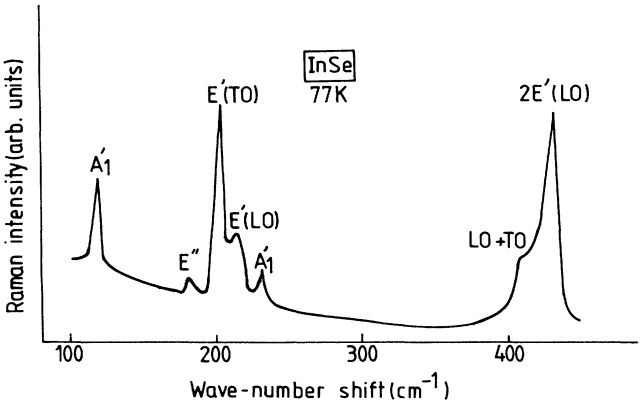

FIG. 3. Unanalyzed resonance Raman spectrum of InSe using the $\lambda=4880$ Å line of an argon-ion laser at 77 K.

213, 412, and 430 cm^{-1} are the polar modes. It is well known from theory[24,25] that, though the polar phonons are forbidden by the selection rules in polar semiconductors, these modes become active with large enhancement in intensity when the incident energy approaches the resonance. InSe is a polar semiconductor and shows that polar modes are present only near resonance, whereas the nonpolar modes are allowed by selection rules in the Raman scattering, off resonance.

A. Nonpolar modes

The modes observed in InSe at 118, 180, and 230 cm^{-1} are the nonpolar phonons. Figure 4 shows the resonant Raman spectra of InSe at 77 K with incident energies varying from 2.41 to 2.60 eV. The frequencies of these modes increase by a few cm^{-1} as the temperature is lowered from 300 to 77 K.

As the laser energy varies away from resonance to the excitonic energy, these nonpolar modes show continuous resonance enhancement. This is clear from Figs. 4(a)–4(c), where the three nonpolar modes show continuous enhancement in their intensities until just below the excitonic energy. At very near to excitonic energy, as shown in Fig. 4(d), the intensities of the nonpolar modes

TABLE I. Frequencies of various phonons in InSe.

Assignment	Frequency (cm^{-1}) $T=300$ K[a]	$T=300$ K[b]	$T=77$ K[b]
A_1'	117	116	118
E''	177	177	180
E'(TO)	199	201	203
E'(LO)	212	210	213
A_1'	226	228	230
Second order	400	401	406
Second order	416	411	412
Second order	423	425	430

[a]Reference 9.
[b]Our results.

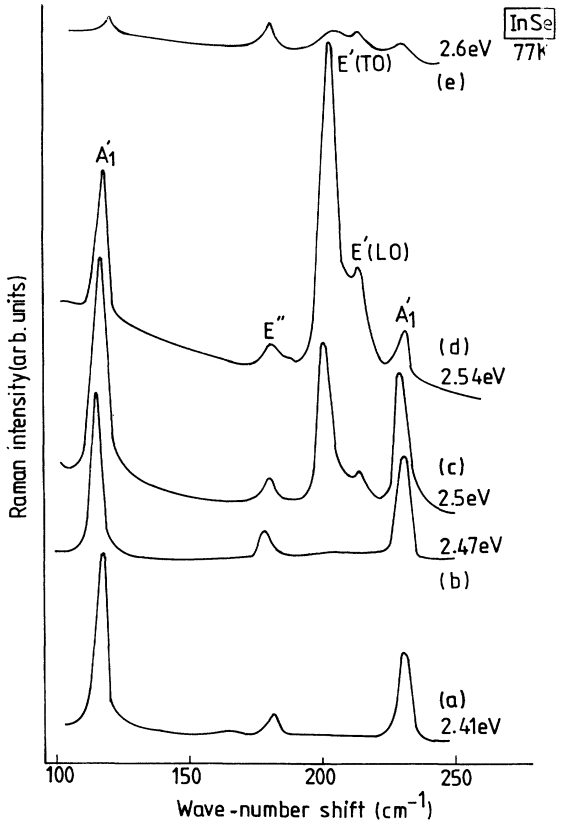

FIG. 4. Unanalyzed resonance Raman spectrum of InSe using different wavelengths of an argon-ion laser at 77 K.

show an apparent decrease. It is to be mentioned here that Fig. 4(d) is the uncorrected Raman spectrum and the absorption coefficient at 2.54 eV is more than that at 2.5 eV. Consequently, the absorption-corrected[5] Raman intensity shows resonance exactly at 2.54 eV.

B. Polar modes

The modes of 203 and 230 cm^{-1} are the polar modes. They are assigned to E'(TO) and E'(LO) modes of ε-polytype[9] InSe. The E'(LO) mode is ir and Raman active and cannot be accounted for if one assumes β-polytype. Figure 5(c) shows the Raman spectrum excited with $\lambda=4965$ Å. In this figure one can see the sudden appearance of the polar modes E'(TO) and E'(LO). Here the laser-beam energy (2.5 eV) approaches E_1' exciton energy (2.535 eV) from the lower-energy side, and hence the Raman-scattering efficiency increases rapidly. A similar observation was made by Kuroda and Nishina[11,13] in γ-polytype InSe. In their ir measurements it was found that the energy of the weaker component of the pair (the weak mode at 213 cm^{-1} in Fig. 4) was close to that of the forbidden Γ_3^1(LO) mode. From this and from the asymmetric nature of the mode, they attributed this mode to the LO-phonon scattering assisted by emission and/or absorption of either the TA or LA mode of acoustic phonons.

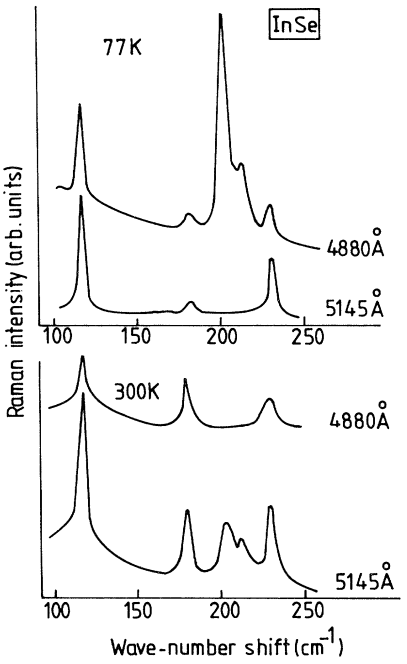

FIG. 5. Near-resonance Raman spectra of $\lambda=5145$ Å at 300 K and for $\lambda=4880$ Å at 77 K. Off-resonance Raman spectra for $\lambda=5145$ Å at 77 K and for $\lambda=4880$ Å at 300 K.

Figure 5 shows two examples of near-resonance spectra: one excited by the 5145-Å line of the argon-ion laser at 300 K and the other by the 4880-Å line at 77 K. The 5145-Å line is about 10 meV in energy below the E_1' exciton, and the 4880-Å line is 5 meV above at the respective temperatures. It is to be mentioned here that the polar modes vanish fast for laser energies away from resonance. Hence the data acquired would be insufficient to plot a realistic resonance curve. The resonant behavior at 200 and 230 cm^{-1} can easily be reconcilde with predictions of Martin[24] and the experimental observations[26,27] reported on forbidden modes. That is, near resonance when q-dependent scattering predominates, infrared active modes that are normally forbidden can become Raman active. In InSe the E'(LO) and E'(TO) phonon modes are examples of forbidden phonon modes that become active when resonance is approached and q-dependent scattering predominates. Such a selection-rule breakdown has also been predicted by Martin[24] and observed previously[26,27] in other compounds.

The Raman efficiency is evaluated with corrections for absorption by taking absorption data from published work.[5]

The resonance curves for the three nonpolar modes at 117, 180, and 230 cm^{-1} are plotted in Figs. 6, 7, and 8, respectively. In order to thoroughly study the resonance, the Raman spectrum was recorded using argon-ion laser lines and temperature tuning the gap. By varying the temperature between 300 and 77 K, it was possible to tune the exciton gap from 2.42 to 2.535 eV.

Kuroda and Nishina[11] have reported the resonance behavior of nonpolar modes. In order to explain their results, they used the usual theory of Zeyher, Ting, and Birman[14] and attributed the E_1' excitonic peak in InSe to three-dimensional M_0 excitons. However, these authors have not considered the effect of dimensionality on the M_1 edge, which would be reflected in a resonant Raman experiment. The excitonic continuum as well as the bound states should be involved in the process as the resonant intermediate states. Their experimental results (Fig. 2 of Ref. 11) did not show double-resonance behavior.

A careful examination of their results would show that the number of experimental points in the region of our in-

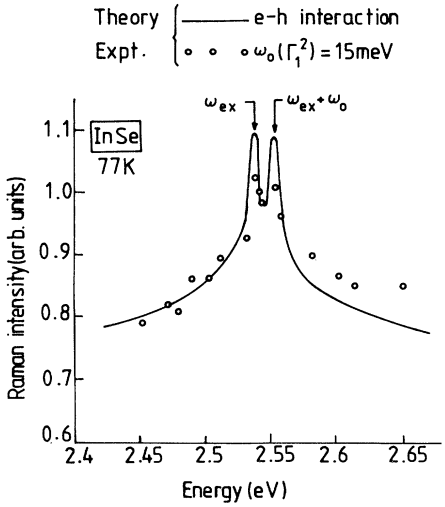

FIG. 6. Resonance curve of InSe at 77 K for $h\omega_0=15$ meV. The solid line shows the e-h interaction using Eqs. (40) and (41), taking $h\omega_g=2.88$ eV, $|E_1(0)|=0.345$ eV, and $\Gamma=5$ meV. The open circles represent the experimental points. The Raman intensity is plotted on a $\log_{10}$ scale.

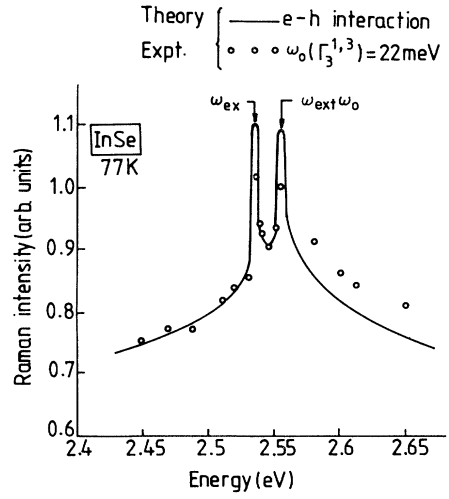

FIG. 7. Resonance curve of InSe at 77 K for $h\omega_0=22$ meV. Other parameters are same as in Fig. 6.

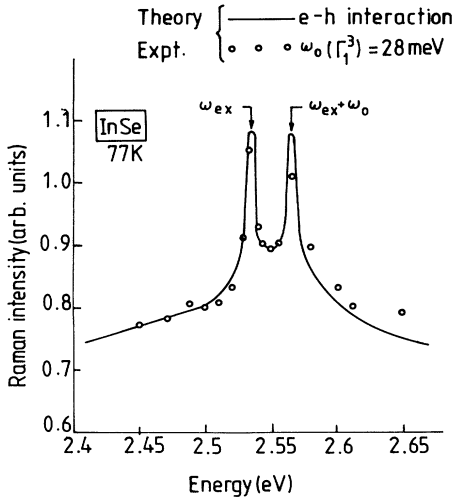

FIG. 8. Resonance curve of InSe at 77 K for $\hbar\omega_0=28$ meV. Other parameters are same as in Fig. 6.

terest, viz., 2.52–2.60 eV, are too few. Hence it is possible that the fine structure of double resonance would have been missed and because of which their resonance peak appears highly asymmetric. Based on the asymmetry and apparent antiresonance seen in their results, they chose a hydrogenic M_0 exciton as the intermediate state, whereas the absorption measurements of Abutalybov and Belle[6] clearly identified the formation of hyperbolic excitons near the M_1 saddle point. Furthermore, in GaSe,[28] which is similar to InSe in many respects, a double resonance is observed.

In our experiments and theory, we have concentrated on the problem of exploring the resonant nature of the E_1' energy gap. We have formulated an approximate theory to calculate the Raman amplitude at the M_1 edge in two dimensions, both for free *e-h* pairs as well as for Coulomb correlated pairs as intermediate scattering states. A detailed discussion of the theory is given in Sec. III.

Together with the experimental points, our theoretical predictions of the resonance behavior has also been plotted in Figs. 6–8 for the nonpolar phonon modes. The solid line is plotted using the above equations [Eqs. (40) and (41)], taking $\hbar\omega_g=2.88$ eV, $\epsilon=6.5$, $\hbar\Gamma=0.006$ eV, $K=1$, and $|E_1(0)|=0.345$ eV for interacting *e-h* pairs, which shows the double-resonance behavior corresponding to incident- and scattered-photon energies equal to the E_1' excitonic energy. Experimentally, also, we have observed the double resonance which matches well with our theory. Dimensionality plays an important role in the Raman-scattering process, which is clear from the excellent agreement of the experimental and theoretical results. From the results obtained in this study, we contend that metastable (hyperbolic) excitons at the M_1 edge act as intermediate scattering states in the Raman process.

VI. CONCLUSIONS

We have presented a detailed theory of resonant Raman scattering near the critical points in two-dimensional semiconductors. A representative sample from a quasi-two-dimensional layered semiconductor was chosen for the experiments, emphasizing the dimensionality-related aspect of the RRS process.

For two-dimensional semiconductors, the Raman amplitude is calculated at M_0 and M_1 singularities for free as well as interacting *e-h* pairs. The calculated Raman amplitude at all singularities for free *e-h* pairs shows a double-resonance behavior at ω_g and $\omega_g+\omega_0$ corresponding to incoming and outgoing resonances. Double-resonance behavior is also observed near the discrete exciton energies ω_{ex} and $\omega_{ex}+\omega_0$ (ω_0 is the phonon energy) at the M_0 edge for Coulomb interaction between electron-hole pairs leading to a bound state. Furthermore, in addition to this resonance, scattering due to continuum states near the M_0 edge is also observed. At the M_1 critical point, no bound state has been reported previously. The Coulomb interaction between *e-h* pairs gives an adequate description of discrete as well as continuum states. This interaction leads to the existence of metastable (hypberbolic) excitons near the M_1 edge, and the resonance behavior is analogous to that in the M_0 edge with interacting *e-h* pairs.

The experimental resonance curves for nonpolar modes in InSe near the excitonic transition E_1' show a double-resonance structure corresponding to ω_{ex} and $\omega_{ex}+\omega_0$. Earlier workers had interpreted their results based on Raman-scattering theory, considering three-dimensional hydrogenic M_0 excitons as intermediate scattering states. These theories grossly neglect the effect of dimensionality on the M_1 edge, which would be reflected in RRS experiments. The results of our theoretical treatment of the RRS amplitude at the M_1 edge in two dimensions, which considers the excitonic continuum as well as the bound states (hyperbolic excitons), agree well with the aforementioned experimental resonance curves, emphasizing the hyperbolic excitons as the intermediate scattering states. The polar modes of InSe are observed near resonance only. Away from resonance their intensity decreases drastically.

*Formerly, Shalini Mathur.

[1]T. J. Wieting and J. L. Verble, Phys. Rev. B **5**, 1473 (1972).
[2]S. Jandl, J. L. Brebner, and B. M. Powell, Phys. Rev. B **13**, 686 (1976).
[3]J. L. Brebner, S. Jandl, and B. M. Powell, Solid State Commun. **13**, 1555 (1973).
[4]S. Jandl and J. L. Brebner, Can. J. Phys. **52**, 2454 (1974).
[5]M. V. Andriyashik, M. Yu. Sakhnovskii, V. B. Timofeev, and A. S. Yakimova, Phys. Status Solidi **28**, 277 (1968).
[6]G. I. Abutalybov and M. L. Belle, Fiz. Tekh. Poluprovodn. **8**,

2392 (1974) [Sov. Phys. Semicond. **8**, 1559 (1975)].
[7]C. Carlone and S. Jandl, Solid State Commun. **29**, 31 (1979).
[8]N. M. Gasanly, B. M. Yavadov, V. I. Tagirov, and E. A. Vinogradov, Phys. Status Solidi B **89**, K43 (1978).
[9]S. Jandl and C. Carlone, Solid State Commun. **25**, 5 (1978).
[10]N. Kuroda and Y. Nishina, Solid State Commun. **30**, 95 (1979).
[11]N. Kuroda and Y. Nishina, Solid State Commun. **28**, 439 (1978).
[12]N. Kuroda, I. Munakata, and Y. Nishina, J. Phys. Soc. Jpn. **51**, 839 (1982).
[13]N. Kuroda and Y. Nishina, Solid State Commun. **34**, 481 (1980).
[14]R. Zeyher, C. S. Ting, and J. L. Birman, Phys. Rev. B **10**, 1725 (1974).
[15]B. Bendow and J. L. Birman, Phys. Rev. B **1**, 1678 (1970); **4**, 569 (1971).
[16]K. P. Jain and Gayatri Choudhury, Phys. Rev. B **8**, 676 (1973).
[17]B. Velický and J. Sak, Phys. Status Solidi **16**, 147 (1966).
[18]Shalini Mathur, K. P. Jain, R. K. Soni, C. Julien, and M. Balkanski, Phys. Rev. B **43**, 3952 (1991).
[19]E. O. Kane, Phys. Rev. **180**, 852 (1969).
[20]Leonard I. Schiff, *Quantum Mechanics,* 3rd ed. (McGraw-Hill, New York, 1968).
[21]Masaki Shinada and Satoru Sugano, J. Phys. Soc. Jpn. **21**, 1936 (1966).
[22]Y. Toyozawa, M. Inoue, T. Inui, M. Okazaki, and E. Hanamura, J. Phys. Soc. Jpn. **22**, 1337 (1967).
[23]B. A. Weinstein and M. Cardona, Phys. Rev. B **8**, 2795 (1973).
[24]R. M. Martin, Phys. Rev. B **4**, 3676 (1971).
[25]R. M. Martin and T. C. Damen, Phys. Rev. Lett. **26**, 86 (1971).
[26]E. Anastassakis and E. Burstein, in *Proceedings of the Second International Conference on Light Scattering in Solids,* edited by M. Balkanski (Flammarion, Paris, 1971).
[27]P. F. Williams and S. P. S. Porto, Phys. Rev. B **8**, 1782 (1973).
[28]J. Reydellet and J. M. Besson, Solid State Commun. **17**, 23 (1975).